Available online at www.sciencedirect.com
SCIENCE DIRECT®
Journal of Solid State Chemistry 178 (2005) 28–35
JOURNAL OF SOLID STATE CHEMISTRY
www.elsevier.com/locate/jssc

Synthesis, crystal structure and magnetic properties of the spin ladder compounds $La_2(Cu_{1-x}Zn_x)_2O_5$ and $La_8(Cu_{1-x}Zn_x)_7O_{19}$

C. Sekar[a,*], B. Schüpp-Niewa[a], G. Krabbes[a], M. Wolf[a], D. Eckert[a], M. Knapp[b], K.-H. Müller[a]

[a]*Leibniz-Institut für Festkörper- und Werkstoffforschung Dresden (IFW), Postfach 270116, 01171 Dresden, Germany*
[b]*TU Darmstadt, Fachbereich Material- und Geowissenschaften, Petersenstr. 23, 64287 Darmstadt, Germany*

Received 23 July 2004; received in revised form 4 October 2004; accepted 6 October 2004

Abstract

The influence of Zn-doping on the crystal structure and magnetic properties of the spin ladder compounds $La_2Cu_2O_5$ (4-leg) and $La_8Cu_7O_{19}$ (5-leg) have been investigated. The $La_2(Cu_{1-x}Zn_x)_2O_5$ and $La_8(Cu_{1-x}Zn_x)_7O_{19}$ solid solutions were obtained as single phases with $x = 0-0.1$ via the solid-state reaction method in the temperature range between 1005–1010 °C and 1015–1030 °C in oxygen and air atmospheres, respectively. The lattice parameters a and c of the monoclinic crystal structures as well as the unit cell volume V increase with increasing x, while b and β decrease for both series. The magnetic susceptibilities χ of both series show a very similar behavior on temperature as well as on Zn-doping, which is supposed to be due to the similar Cu–O coordination in both $La_2Cu_2O_5$ and $La_8Cu_7O_{19}$. For low Zn-doping ($x \leqslant 0.04$), a spin-chain like behavior is found. This quasi-one-dimensional behavior is strongly suppressed in both series for $x \geqslant 0.04$. Here, the maximum (characteristic for spin chains) in $\chi(T)$ disappears and $\chi(T)$ decreases monotonically with increasing temperature.

Keywords: Lanthanum cuprate; Spin ladders; Zn-doping; Crystal structure; Magnetic susceptibility

1. Introduction

The study of spin ladder systems has attracted considerable attention because of possible relevance to the mechanism of high-T_c superconductivity. Such a ladder structure is made of n linear Cu–O–Cu chains (legs) linked with each other via the ''rungs'' forming two-dimensional Cu_2O_3 sheets. These ladders are magnetically separated from each other due to inter-ladder 90° Cu–O–Cu bonds causing spin frustration at the ladder boundary. The magnetic properties of the spin ladders depend on the number of legs. It has been predicted that the even-leg ladders should reveal two important features of high-T_c superconductivity; (i) the existence of a spin gap, and thereby a magnetic susceptibility vanishing with decreasing temperature and (ii) the possibility of superconductivity when slightly doped with holes. On the other hand, the susceptibility of ladders with an odd number of legs is predicted to remain finite for vanishing temperatures [1]. Experimental studies have been performed only on a few spin ladder compounds; $Sr_{n-1}Cu_{n+1}O_{2n}$ ($n = 3, 5$) [2,3], (La,Sr)$CuO_{2.5}$ [4], $(Sr_{1-x}Ca_x)_{14}Cu_{24}O_{41}$ [5], $La_{4+4n}Cu_{8+2n}O_{14+8n}$ ($n = 2, 3$) [6–8]. Among these, $Sr_{n-1}Cu_{n+1}O_{2n}$ ($n = 3, 5$) is a unique series which allows both 2-leg ($SrCu_2O_3$) and 3-leg ($Sr_2Cu_3O_5$) ladders with structures made of ideal 2D Cu_2O_3 sheets. These two compounds are treated as prototypes to investigate the difference in magnetism between even- and odd-leg ladders and, indeed the theoretical predictions concerning magnetism have been confirmed [3]. The compounds $SrCu_2O_3$ and $Sr_2Cu_3O_5$ could be synthesized only under high pressure and carrier doping is not possible.

*Corresponding author.
E-mail address: sekar2025@yahoo.co.in (C. Sekar).

0022-4596/$ - see front matter © 2004 Elsevier Inc. All rights reserved.
doi:10.1016/j.jssc.2004.10.012

Therefore, the research has been confined to magnetism with these materials. The other well-known two-leg ladder material $(La_{1-x}Sr_x)CuO_{2.5}$ (Space group: *Pbam* (No. 55)) is also a high-pressure phase [4]. It does not become superconducting (down to 5 K) even after substantial hole-doping. So far, $(Sr_{1-x}Ca_x)_{14}Cu_{24}O_{41}$ (2-leg) is the only ladder material which becomes superconducting with $T_c = 12$ K under high pressure of 3.5 GPa [9]. This phase can be synthesized in ambient pressure; large single crystals could be grown with controlled carrier doping. The compounds $La_2Cu_2O_5$ and $La_8Cu_7O_{19}$, $n = 2, 3$ members of the new homologous series of lanthanum cuprate $La_{4+4n}Cu_{8+2n}O_{14+8n}$, are promising candidates for 4- and 5-leg ladders, respectively [6–8]. Both compounds crystallize in the monoclinic space group $C2/c$ (No. 15). These compounds can be synthesized only in a narrow temperature range. Single crystals of both systems were grown by modified flux method, and hole doping was attempted via high-oxygen-pressure annealing process [7,10]. Although the electrical resistivity decreased significantly, no change of semiconducting behavior was observed. Further annealing resulted in the decomposition of $La_2Cu_2O_5$ into structurally distorted perovskite $LaCuO_{3-\delta}$ [11].

The compounds $La_2Cu_2O_5$ and $La_8Cu_7O_{19}$ consist of both spin ladder blocks (4- and 5-leg) which are formed by Cu^{2+} ions coupled by almost 180° Cu–O–Cu bonds both along the leg and rung directions, and Cu_2O_6 blocks which connect each ladder perpendicular to the ladder plane. The magnetic sucsceptibility in these compounds mostly come from the Cu_2O_6 blocks. Therefore, it is very difficult to distinguish a magnetic contribution purely originating from the spin-ladders. Here, doping nonmagnetic Zn^{2+}-ions into $La_2(Cu_{1-x}Zn_x)_2O_5$ and $La_8(Cu_{1-x}Zn_x)_7O_{19}$ ($x = 0.0-0.1$) can be expected to affect the magnetic properties in various fashions depending on the site preference and concentration of Zn. Moreover, it is not yet clear how the magnetic properties of the spin ladders evolve with increasing the number of legs. In this paper, we report the influence of Zn-doping on preparation, crystal structure, and magnetic properties of the 4-leg ($La_2Cu_2O_5$) and 5-leg ($La_8Cu_7O_{19}$) ladder compounds.

2. Experimental

2.1. Synthesis, thermal and magnetic measurements

Polycrystalline samples of $La_2(Cu_{1-x}Zn_x)_2O_5$ and $La_8(Cu_{1-x}Zn_x)_7O_{19}$ ($x = 0-0.1$) were prepared via solid-state reactions of La_2O_3 (MaTeck 99.99%, dried in air at 850 °C for 15 h), CuO (MaTeck 99.99%), and ZnO (Chempure 99.9%). The powders with appropriate molar ratios were thoroughly mixed in agate mortar. The mixtures were placed in alumina boats and loaded into furnaces preheated to temperatures between 1005–1010 °C ($La_2(Cu_{1-x}Zn_x)_2O_5$), and 1015–1030 °C ($La_8(Cu_{1-x}Zn_x)_7O_{19}$) in oxygen and air atmospheres, respectively. After 1-day sintering, the products were quenched to room temperature. This process was continued for 5 days with intermediate grindings. The final products were confirmed to be single-phase ceramic samples according to the powder X-ray diffraction and thermal analyses.

Thermogravimetry-Differential thermal analysis (TG-DTA) was carried out by measuring weight loss and calorimetric signals from room temperature to 1200 °C with a heating rate of 10 K/min in both oxygen and air atmospheres using simultaneous symmetrical thermo-analyser TAG 16 (SETARAM).

The dc magnetic susceptibility χ of all compounds was determined from $\chi = M/H$ in the temperature range from 4 to 400 K, where the magnetization M was measured in a SQUID magnetometer at an applied field $\mu_0 H = 1$ T.

2.2. X-ray powder diffraction (XRD) measurements

XRD patterns were taken on an X'Pert diffractometer 3040/00 (Philips) using Co-$K\alpha$ radiation. The $La_2(Cu_{1-x}Zn_x)_2O_5$ and $La_8(Cu_{1-x}Zn_x)_7O_{19}$ samples were mixed with silicon powder as an internal standard and prepared with ethanol in PVC sample holders. The X-ray data were collected in the diffraction angle range from 10° to 130° (2θ) with a step width of $\Delta(2\theta) = 0.03°$. The phase identification was carried out with the program X'PERT HIGHSCORE 1.0a (Philips) [12]. The lattice parameters were calculated using the following two methods: (1) The peak positions were extracted by profile fitting with PROFIT 1.0 (Philips) [13]. After correction, according to the peak positions of the Si standard, the unit cell parameters were refined with the program UNITCELL [14]. (2) Rietveld refinements of the X-ray powder diffraction patterns were carried out using the lattice parameter $a = 5.4309$ Å for the silicon standard with the program X'PERT PLUS (Philips) [15]. Positional and displacement parameters were taken from literature [6,8]. These values were not allowed to vary.

Temperature-dependent XRD measurements on $La_2(Cu_{1-x}Zn_x)_2O_5$ and $La_8(Cu_{1-x}Zn_x)_7O_{19}$ powders were performed with synchrotron radiation at the beamline B2, Hasylab, DESY, Hamburg. For high-temperature measurements a STOE high-temperature chamber for Debye–Scherrer geometry was used. Diffraction patterns were recorded using the OBI detector in the range of $10° \leqslant 2\theta \leqslant 50°$, $\lambda = 0.699352$ Å, $\Delta T = 40$ K. The samples were prepared in quartz capillaries ($\varnothing_{\text{outside}} = 0.3$ mm) in air, closed by quartz glass filaments. The unit cell parameters were refined with

the Rietveld method using the program X'PERT PLUS (Philips) [15]. For low-temperature measurements on $La_8(Cu_{1-x}Zn_x)_7O_{19}$ a closed-cycle He-cryostat was used. The powders were prepared on a Si single-crystal holder. XRD patterns of $La_8(Cu_{1-x}Zn_x)_7O_{19}$ with $x = 0$, 0.04 and 0.1 were recorded in high-resolution geometry in selected diffraction ranges ($12.5^\circ \leqslant 2\theta \leqslant 15.5^\circ$ and $17.5^\circ \leqslant 2\theta \leqslant 22^\circ$), $\lambda = 0.709621$ Å. The unit cell parameters were refined with the program FULLPROF [16].

3. Results and discussion

3.1. Synthesis and thermal stability

In accordance with Cava et al. [6], the single-phase compounds $La_2Cu_2O_5$ and $La_8Cu_7O_{19}$ could be synthesized in oxygen and air at 1005 and 1015 °C, respectively. Here, loading the starting mixtures into preheated furnace and further quenching after sintering are necessary to avoid the formation of La_2CuO_4. If La_2CuO_4 has formed first during the chemical reaction, the target compounds are not obtained. In order to monitor the phase formation and substitution of Zn for Cu in $La_2Cu_2O_5$ and $La_8Cu_7O_{19}$, we have carried out thermal analyses of all samples investigated in the present work. The TG-DTA profile of undoped $La_2Cu_2O_5$ and $La_8Cu_7O_{19}$ samples measured in oxygen atmosphere are shown in Fig. 1. The DTA curve of $La_2Cu_2O_5$ shows two endothermic peaks at 1065 and 1090 °C, respectively, with a total weight loss of 1.1% oxygen suggesting that $La_2Cu_2O_5$ decomposes into $La_8Cu_7O_{19}$ and CuO at 1065 °C and the further reaction at 1090 °C corresponds to the decomposition of $La_8Cu_7O_{19}$ into La_2CuO_4 and liquid CuO. Powder XRD studies of the final product obtained after endothermic event at 1090 °C revealed that the decomposition products are a mixture of La_2CuO_4, $La_8Cu_7O_{19}$, $La_2Cu_2O_5$, and CuO. The results are in qualitative agreement with the phase diagram of the La_2O_3–CuO system [8]. For $La_2(Cu_{1-x}Zn_x)_2O_5$ ($x = 0-0.1$) samples, the intensity of the endothermic peak at 1065 °C decreases with increase in Zn-content and disappears for $x = 0.1$. Instead of two peaks, one broad peak appears at an increased temperature of 1102 °C. The DTA profile of $La_8Cu_7O_{19}$ shows a sharp endothermic peak at 1082 °C which corresponds to the peritectic decomposition of $La_8Cu_7O_{19}$ into La_2CuO_4 and liquid CuO. All $La_8(Cu_{1-x}Zn_x)_7O_{19}$ ($x = 0-0.1$) samples showed only one peak and the decomposition temperature increases with increasing Zn-content. The composition of $La_8(Cu_{1-x}Zn_x)_7O_{19}$ samples, sintering temperatures, and decomposition temperatures (in both oxygen and air) are compiled in Table 1. A homogenous doping of Zn within the sample in both the series can be concluded from these results.

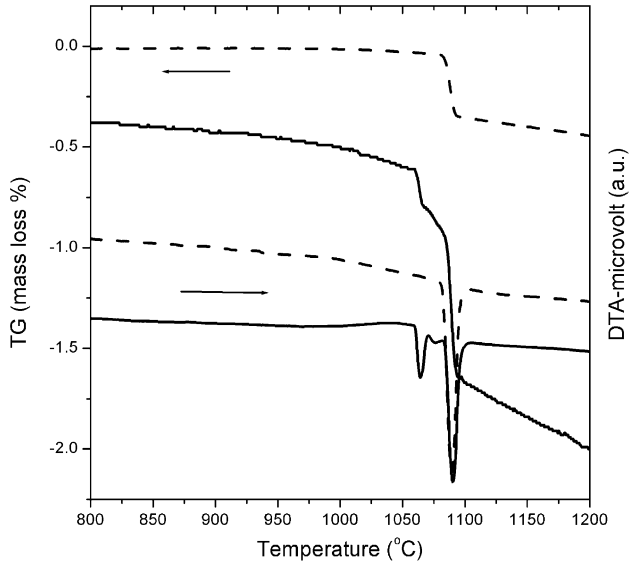

Fig. 1. DTA–TG profiles of $La_2Cu_2O_5$ (solid line) $La_8Cu_7O_{19}$ (dotted line) at $p(O_2) = 1$ bar.

3.2. Structural analyses

3.2.1. Crystal structure of $La_{4+4n}Cu_{8+2n}O_{14+8n}$ (n=2,3)

The compounds $La_2Cu_2O_5$ and $La_8Cu_7O_{19}$ crystallize in the monoclinic space group $C2/c$ (No. 15) [6–8]. The crystal structures are shown in Fig. 2a. The Cu–O

Table 1
Preparation conditions and decomposition temperatures of $La_8(Cu_{1-x}Zn_x)_7O_{19}$ in oxygen and air atmospheres

$La_8(Cu_{1-x}Zn_x)_7O_{19}$ (x)	Preparation temp. (°C) (air)	Decomposition temp. (°C) (oxygen)	Decomposition temp. (°C) (air)
0	1015	1082	1038
0.01	1015	1086	1042
0.02	1015	1087	1045
0.04	1015	1088	1045
0.06	1020	1090	1047
0.08	1025	1092	1053
0.10	1030	1094	1056

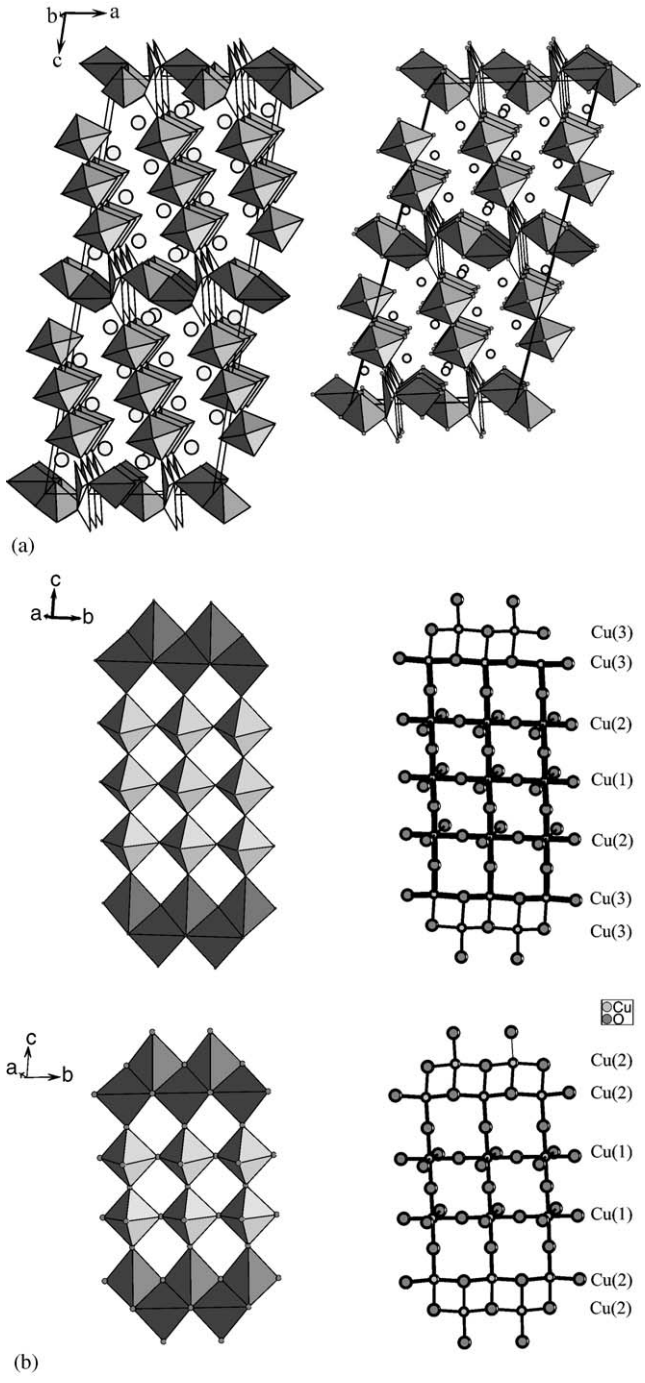

Fig. 2. (a) Crystal structures of $La_8Cu_7O_{19}$ (left) and $La_2Cu_2O_5$ (right) (bright circles: lanthanum; in the middle of the polyhedra: copper; polyhedra vertices: oxygen). (b) Ladder Cu–O sub-structure of $La_8Cu_7O_{19}$ and $La_2Cu_2O_5$: left: polyhedra presentation, right: ball and stick model.

sub-structure contains infinite ribbons, which can be described as perovskite-type layers consisting of $n = 2$ ($La_2Cu_2O_5$) or $n = 3$ ($La_8Cu_7O_{19}$) Jahn–Teller elongated octahedra and two additional Cu–O planes of complex geometry. The complex Cu–O planes consist of two sub-units. $(CuO_2)_x$-chains, consisting of cis-edge-sharing flattened double tetrahedra, terminating the $n = 2$ and 3 ribbons. The rows of flattened tetrahedra form the "legs", which are interconnected by "rungs" of the ribbon octahedra forming the ladder-like sub-structure. Another type of tetrahedra pairs bridges the end legs of two neighboring ladders, providing a link within the third dimension. Thus $La_2Cu_2O_5$ can be regarded as a 4-leg and $La_8Cu_7O_{19}$ as a 5-leg ladder compound as is shown in Fig. 2b. It can be noticed that the ladder structures are made of two (Cu(1):octahedral environment, Cu(2): tetrahedral environment), and three (Cu(1) and Cu(2): octahedral environment, Cu(3): tetrahedral environment) different Cu-sites of $La_2Cu_2O_5$ and $La_8Cu_7O_{19}$, respectively. For detailed information about the structure refinement of $La_8Cu_7O_{19}$ see [8].

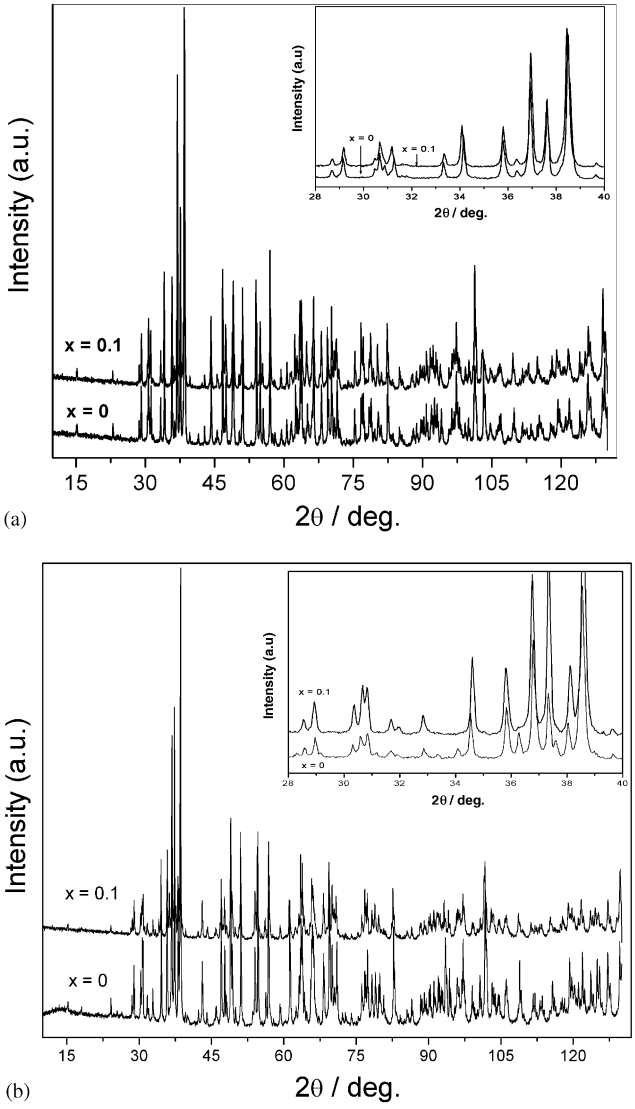

Fig. 3. Powder XRD patterns of (a) $La_2(Cu_{1-x}Zn_x)_2O_5$ and (b) $La_8(Cu_{1-x}Zn_x)_7O_{19}$. Polycrystalline samples measured at room temperature; inset: a part of the XRD patterns are expanded for better clarity.

Table 2
Lattice parameters of (a) $La_2(Cu_{1-x}Zn_x)_2O_5$ and (b) $La_8(Cu_{1-x}Zn_x)_7O_{19}$ calculated from the room temperature XRD patterns using the programs UNITCELL and X'PERT PLUS (Rietveld method)

Method of lattice parameter calculation	x	a(Å)	b(Å)	c(Å)	β(deg)	V(Å)^3
(a)						
UnitCell	0.00	13.8727(3)	3.7494(1)	27.9658(6)	106.049(2)	1397.94(3)
UnitCell	0.01	13.8732(2)	3.7492(1)	27.9695(4)	106.016(1)	1398.33(3)
UnitCell	0.02	13.8751(2)	3.7489(1)	27.9725(5)	105.996(1)	1398.70(3)
UnitCell	0.05	13.8765(3)	3.7483(1)	27.9833(5)	105.929(1)	1399.60(4)
UnitCell	0.10	13.8797(3)	3.7483(1)	27.9969(4)	105.846(2)	1401.21(3)
Rietveld	0.00	13.8725(3)	3.74915(8)	27.9648(6)	106.050(2)	1397.76
Rietveld	0.01	13.8740(3)	3.74918(8)	27.9678(6)	106.027(2)	1398.24
Rietveld	0.02	13.8756(3)	3.74874(7)	27.9712(5)	105.999(2)	1398.60
Rietveld	0.05	13.8773(3)	3.74839(8)	27.9823(5)	105.937(2)	1399.62
Rietveld	0.10	13.8808(3)	3.74789(8)	27.9978(6)	105.843(2)	1401.22
(b)						
UnitCell	0.00	13.8351(3)	3.7598(1)	34.6057(5)	99.340(2)	1776.21(4)
UnitCell	0.04	13.8377(3)	3.7590(1)	34.6255(8)	99.246(2)	1777.67(5)
UnitCell	0.06	13.8383(3)	3.7594(1)	34.6334(5)	99.205(2)	1778.56(4)
UnitCell	0.08	13.8399(3)	3.7590(1)	34.6437(6)	99.171(2)	1779.26(4)
UnitCell	0.10	13.8439(3)	3.7582(1)	34.6470(7)	99.156(2)	1779.67(5)
Rietveld	0.00	13.8347(3)	3.75978(8)	34.6040(6)	99.332(2)	1776.12
Rietveld	0.04	13.8375(3)	3.75935(9)	34.6257(8)	99.243(2)	1777.85
Rietveld	0.06	13.8387(3)	3.75953(9)	34.6367(8)	99.205(2)	1778.83
Rietveld	0.08	13.8405(3)	3.75931(9)	34.6479(8)	99.168(2)	1779.72
Rietveld	0.10	13.8442(4)	3.7581(1)	34.649(1)	99.156(3)	1779.77

The estimated standard deviations (ESD) of the last significant digit are given in parentheses.

3.2.2. *X-ray powder diffraction studies at room temperature*

X-ray powder diffraction patterns for the extreme concentrations ($x = 0, 0.1$) of $La_2(Cu_{1-x}Zn_x)_2O_5$ and $La_8(Cu_{1-x}Zn_x)_7O_{19}$ are shown in Fig. 3a and b, respectively. $La_2(Cu_{1-x}Zn_x)_2O_5$ ($x = 0-0.1$) samples are single phase except for a small amount of residual CuO. $La_8(Cu_{1-x}Zn_x)_7O_{19}$ samples with $x = 0.0$, 0.04 are single phase, according to phase analysis by X-ray diffraction, whereas the sample with $x = 0.6$, 0.8, 0.1 prepared at 1015 °C contained traces of $La_2Cu_2O_5$ and La_2CuO_4. However, a slight increase of the sintering temperature (1020–1030 °C) leads to the formation of a single-phase product.

The lattice parameters of the $La_2(Cu_{1-x}Zn_x)_2O_5$ and $La_8(Cu_{1-x}Zn_x)_7O_{19}$ ($x = 0-0.1$) type compounds are summarized in Table 2a and b. The values obtained by different refinement methods are in good agreement. As can be seen in Fig. 4, the lattice parameters a, c and the unit cell volume V increase monotonically with increasing Zn-doping for both systems, whereas the lattice parameter b and the monoclinic angle β decrease. According to Shannon [17], the ionic radii of Cu^{2+} and Zn^{2+} ions are as follows: for coordination number CN = 4 (tetrahedral environment): $r(Zn^{2+}) = 0.60$ Å, $r(Cu^{2+}) = 0.57$ Å; for CN = 6 (octahedral environment): $r(Zn^{2+}) = 0.74$ Å, $r(Cu^{2+}) = 0.73$ Å. Based on the results, it is plausible to assume that, initially ($x \leqslant 0.04$) the Zn-ions replace the tetrahedral Cu-sites (Cu(3) for $La_2Cu_2O_5$ and Cu(4) for $La_8Cu_7O_{19}$). With increasing Zn-concentration ($x \geqslant 0.04$), Zn-ions occupy the other tetrahedral Cu-sites (Cu(2) for $La_2Cu_2O_5$ and Cu(3) for $La_8Cu_7O_{19}$), which are actually coupled to the octahedral ribbons. A proof of this cannot be given by X-ray measurement due to approximately equal atomic scattering factors of Cu and Zn.

3.2.3. *Temperature-dependent XRD studies*

High-temperature XRD measurements were performed on $La_2(Cu_{1-x}Zn_x)_2O_5$ ($x = 0$, 0.1) and $La_8(Cu_{1-x}Zn_x)_7O_{19}$ ($x = 0$, 0.04, 0.1). The lattice parameters a, b, c and the volumes V show a linear increase with increasing temperature up to 833 K ($La_8Cu_7O_{19}$), 793 K ($La_8(Cu_{1-x}Zn_x)_7O_{19}$, $x = 0.04$, 0.1) and 753 K ($La_2(Cu_{1-x}Zn_x)_2O_5$, $x = 0$, 0.1), respectively. At higher temperatures also linear behavior with temperature is observed, but with a different slope. As an example of this behavior, the high-temperature variation of c for $La_8(Cu_{1-x}Zn_x)_7O_{19}$ is presented in Fig. 5a.

The thermal expansion coefficients α_X of the lattice parameters and the unit cell volumes of the studied compounds are calculated according to the

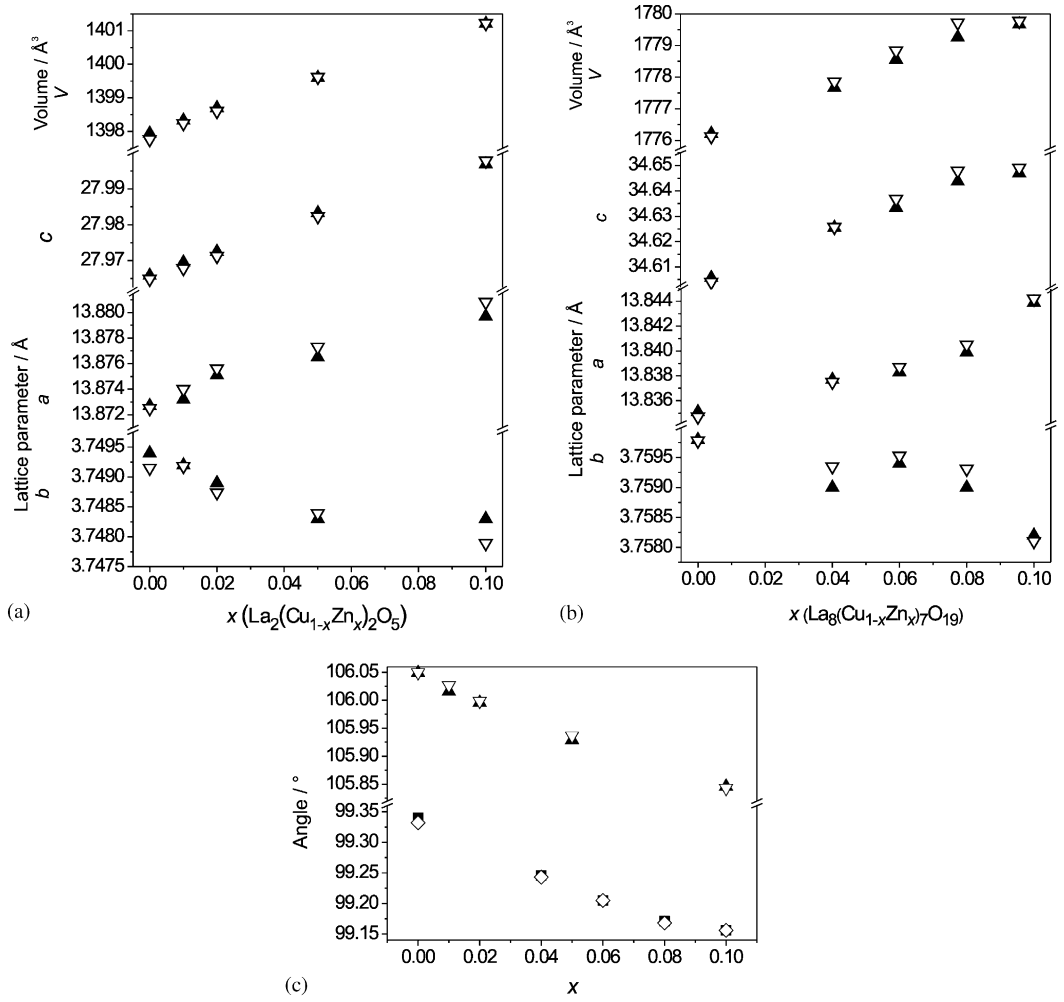

Fig. 4. Lattice parameters of (a) $La_2(Cu_{1-x}Zn_x)_2O_5$ and (b) $La_8(Cu_{1-x}Zn_x)_7O_{19}$ calculated with the programs UNITCELL (▲) and X'PERT PLUS (Rietveld method, X). (c) Unit cell angle ($La_2Cu_2O_5$: triangles, $La_8Cu_7O_{19}$: rhombuses; open symbols: X'PERT PLUS, filled symbols: UNITCELL).

formula

$$\alpha_X = \frac{\Delta X}{X_0 \Delta T} = \frac{X_1 - X_0}{X_0(T_1 - T_0)}, \quad (1)$$

where X_0 and X_1 are the lattice parameters *a, b, c* and the unit cell volume V at temperatures T_0 and T_1, respectively. Table 3 shows the calculated thermal expansion coefficients of all samples. A comparison of the thermal expansion coefficients for $La_8(Cu_{1-x}Zn_x)_7O_{19}$ samples leads to a value of α_a, which is significantly larger than those expansion coefficients of the lattice parameters b (α_b) and c (α_c). The thermal expansion coefficients for all samples behave as follows: $\alpha_a > \alpha_c > \alpha_b$. An exception is $La_8(Cu_{1-x}Zn_x)_7O_{19}$ with $x = 0.1$ in the temperature range of 833 K $\leqslant T \leqslant$ 993 K, and $\alpha_c > \alpha_a > \alpha_b$ (see Table 3 and Fig. 5b). While the α_a of all the investigated samples decreases with increasing Zn content, the thermal expansion coefficients α_b and α_c increase with increasing Zn content between $x = 0.04$ and 0.1. At the temperatures where the different slope of

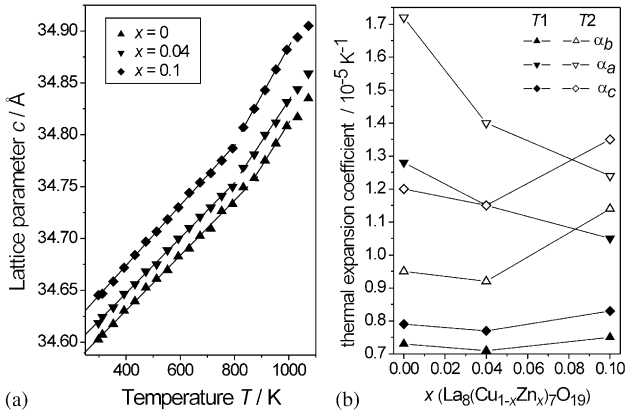

Fig. 5. (a) Dependence of the lattice parameter c of $La_8(Cu_{1-x}Zn_x)_7O_{19}$ on the temperature T according to high-temperature XRD measurements. (b) Thermal expansion coefficients of the lattice parameters of $La_8(Cu_{1-x}Zn_x)_7O_{19}$ ($T1 = 298-793/833$ K, $T2 = 833/873-993$ K).

Table 3
Thermal expansion coefficients of $La_8(Cu_{1-x}Zn_x)_7O_{19}$ and $La_2(Cu_{1-x}Zn_x)_2O_5$

Formula	x	T/K	α_a ($\times 10^{-5}\,K^{-1}$)	α_b	α_c	α_V
$La_8(Cu_{1-x}Zn_x)_7O_{19}$	0	298–833	1.28	0.73	0.79	2.82
		873–993	1.72	0.95	1.20	3.97
	0.04	298–793	1.15	0.71	0.77	2.65
		833–993	1.40	0.92	1.15	3.60
	0.1	298–793	1.05	0.75	0.83	2.67
		833–993	1.24	1.14	1.35	3.80
$La_2(Cu_{1-x}Zn_x)_2O_5$	0	298–753	1.19	0.69	0.80	2.70
		793–993	1.62	0.94	1.12	3.81
	0.1	298–753	1.07	0.73	0.83	2.68
		793–993	1.47	0.93	1.10	3.70

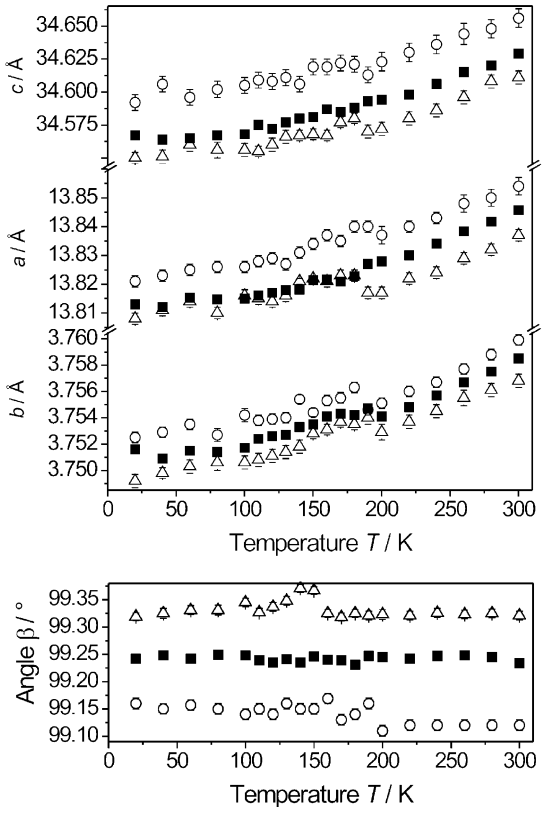

Fig. 6. Temperature dependence of lattice parameters of $La_8(Cu_{1-x}Zn_x)_7O_{19}$ at low temperatures; $x = 0$ (△), $x = 0.04$ (■), $x = 0.1$ (○).

the linear behavior of the thermal expansion occurs, the angle β starts to decrease.

Fig. 6 shows the unit cell parameters calculated from powder diffraction patterns of $La_8(Cu_{1-x}Zn_x)_7O_{19}$ with $x = 0$, 0.04 and 0.1 taken at low temperatures. In the temperature range of $200\,K \leqslant T \leqslant 300\,K$ the lattice parameters of $La_8(Cu_{1-x}Zn_x)_7O_{19}$ decrease linearly with decreasing temperature for all studied compositions. In the temperature range where the magnetic behavior changes drastically (180–200 K) (Section 3.3) a deviation from linear behavior is observed. Especially for the two extreme situations at $x = 0$ and 0.1 an unsteady behavior of the lattice parameters can be detected.

3.3. Magnetic properties

The magnetic susceptibility of both the even-leg $La_2(Cu_{1-x}Zn_x)_2O_5$ and the odd-leg $La_8(Cu_{1-x}Zn_x)_7O_{19}$ ladder compounds are found to be very similar (Figs. 7a and b). At low Zn concentrations (up to $x = 0.02$), $\chi(T)$ shows a flat maximum between 180 and 200 K for both series. This is characteristic for odd-leg spin ladders including simple spin chains; above this temperature χ decreases. At low temperatures χ seems to approach a constant value (the up-turn at lowest temperature is due to minor paramagnetic impurities). For the even-leg ladder compound $La_2(Cu_{1-x}Zn_x)_2O_5$, no hint to the existence of spin gap is found. The described behavior is expected for the 5-leg compound only. Therefore, for small Zn-concentrations, $\chi(T)$ was fitted to an expression describing $\chi(T)$ of a spin chain

$$\chi(T) = CP_{2(y)}/P_{3(y)}/k_BT + C'/K_BT, \quad (2)$$

where $P_2(P_3)$ are certain second (third)-order polynomials of $y = J/k_BT$ [18]. The additional term was

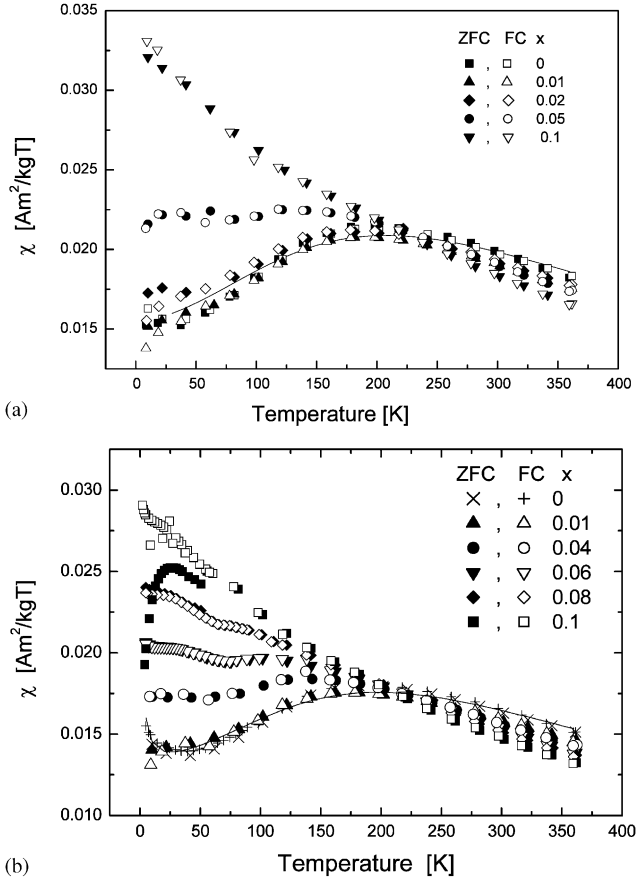

Fig. 7. Temperature dependence of the magnetic susceptibility of (a) $La_2(Cu_{1-x}Zn_x)_2O_5$ and (b) $La_8(Cu_{1-x}Zn_x)_7O_{19}$; The solid lines show the fit ($x = 0$) according to Eq. (2) described in the text.

included in order to describe the up-turn at low temperature. Because of the complex lattice structures of these compounds, the derived J values have to be considered as effective values. J/k_B is about 300 K (320 K) for $La_8Cu_7O_{19}$ ($La_2Cu_2O_5$) and decreases by about 25 K/at% Zn (20 K/at% Zn). From the constant C the following conclusion concerning the Cu^{2+} have been done. From the fit, in the high-temperature limit one Cu^{2+} ion within the chains gives an average contribution of 6.80×10^{-24} Am^2/T (5.52×10^{-24} Am^2/T) for $La_2Cu_2O_5$ ($La_8Cu_7O_{19}$) to C. These values are comparable to the ideal contribution of one Cu^{2+} moment (6.80×10^{-24} Am^2/T). If the Cu^{2+} moments tetrahedrally coordinated, and not linked to ladders, would also contribute to the paramagnetic moment these values should be much larger for both compounds. For example, in $La_8Cu_7O_{19}$, eight of such ions are present per unit cell compared to 20 chain forming ions. It is not yet understood why these tetrahedrally coordinated Cu moments not seem to contribute to χ at high temperature. The average paramagnetic moment decreases with doping, but more strongly than according to a simple dilution law (not shown in the figure here).

Quite surprisingly, for higher doping rates the magnetic behavior changes drastically. The quasi one-dimensional behavior is suppressed for both series above a Zn content of about $x \approx 0.04$ where the maximum in $\chi(T)$ disappears (see Fig. 7a and b). Here, $\chi(T)$ decreases monotonically with increasing temperature T. Whereas initially no differences between field cooling (FC) and zero field cooling (ZFC) curves are observed, also this feature disappears at higher doping rates, e.g. for $x = 0.1$ in $La_8(Cu_{1-x}Zn_x)_7O_{19}$. The similarity in the behavior of both systems might be related to the special structure of the Cu–O ladders, which are different from those of the classical ladder compounds, but similar in the two title compounds. The drastic change in the magnetic behavior on Zn doping is not yet understood. It is an open question, whether the qualitative change in $\chi(T)$ marks a quantum phase transition or, more simply, is related to the minor structural changes observed in this Zn-concentration range as described above.

4. Conclusions

Single phase members of the series $La_2(Cu_{1-x}Zn_x)_2O_5$ and $La_8(Cu_{1-x}Zn_x)_7O_{19}$ ($x = 0-0.1$) have been synthesized. The systematic trends of the lattice parameters of doped samples indicate the possibility of successful substitution of Zn in the parent compounds. Further structural analysis from detailed neutron diffraction studies on similar samples would help in exactly defining the site occupancies of Zn in $La_2Cu_2O_5$ and $La_8Cu_7O_{19}$. Magnetic susceptibility measurements revealed that strong Zn-doping destroys the spin-chain like behavior of both the compounds. For low doping rates, Zn ions cannot be treated as the nonmagnetic dilutions.

Acknowledgments

The authors thank A. Wosylus and R. Gustke for their experimental assistance. This work is supported by a DFG grant (No. KR 1241-3) under the priority program No. 1073.

References

[1] E. Dagato, R.M. Rice, Science 271 (1996) 618.
[2] H. Shaked, Y. Shimakawa, B.A. Hunter, P.G. Radaelli, B. Drabowski, R.L. Hitterman, J.P. Jorgensen, P.D. Han, D.A. Payne, S. Kikkawa, G. Er, F. Kanamura, Phys. Rev. B 50 (1994) 12752.
[3] M. Azuma, Z. Hiroi, M. Takano, Phys. Rev. Lett. 73 (1994) 3463.
[4] Z. Hiroi, M. Takano, Nature 377 (1995) 41.
[5] E.M. McCarron, M.A. Subramanian, J.C. Calabrese, R.L. Harlow, Mater. Res. Bull. 23 (1988) 1355.
[6] R.J. Cava, T. Siegrist, B. Hessen, J.J. Krajewski, W.F. Peck Jr., B. Batlogg, H. Takagi, J.V. Waszczak, L.F. Schneemeyer, J. Solid State Chem. 94 (1991) 170.
[7] C. Sekar, T. Watanabe, A. Matsuda, H. Shibata, Y. Zenitani, J. Akimitsu, J. Solid State Chem. 156 (2001) 422.
[8] B. Schüpp, C. Sekar, W. Gruner, G. Auffermann, C. Bähtz, G. Krabbes, Z. Anorg. Allg. Chem. 630 (2004) 663.
[9] M. Uehara, T. Nagata, J. Akimitsu, H. Takahasi, N. Mori, K. Kinoshita, J. Phys. Soc. Japan 65 (1996) 2764.
[10] C. Sekar, T. Watanabe, A. Matsuda, J. Crystal Growth 212 (2000) 142.
[11] T. Watanabe, C. Sekar, A. Matsuda (unpublished).
[12] X'PERT HIGHSCORE 1.0a, Philips Analytical B.V., Almelo, NL, 2001.
[13] E.J. Sonnefeld, R. Delhez, PROFIT 1.0, Philips Analytical X-ray, Delft, 1996.
[14] T.J.B. Holland, S.A.T. Redfern, UNITCELL, Miner. Mag. 61 (1997) 65.
[15] X'PERT PLUS', Program for Crystallography and Rietveld Analysis, Philips Analytical, 1998–1999.
[16] J. Rodriguez-Carvajal, FULLPROF.2K, Version 1.6, 2000, Laboratoire Léon Brillouin, in: Abstract of Satellite Meeting on Powder Diffraction, Congress of the International Union of Crystallography, Toulouse, France, 1990, p. 127.
[17] R.D. Shannon, Acta Crystallogr. A 32 (1976) 751.
[18] R. Feyerhem, S. Abens, D. Günther, T. Ishida, M. Meißner, M. Meschke, T. Nogami, M. Steiner, J. Phys.: Condens. Matter 12 (2000) 8495.